



Full length article

## Fabrication of dense anisotropic collagen scaffolds using biaxial compression



Jared L. Zitnay<sup>a,b,1</sup>, Shawn P. Reese<sup>a,b,1</sup>, Garvin Tran<sup>a</sup>, Niloofar Farhang<sup>a</sup>, Robert D. Bowles<sup>a,c</sup>, Jeffrey A. Weiss<sup>a,b,c,\*</sup>

<sup>a</sup> Department of Bioengineering, University of Utah, United States

<sup>b</sup> Scientific Computing and Imaging Institute, University of Utah, United States

<sup>c</sup> Department of Orthopaedics, University of Utah, United States

### ARTICLE INFO

#### Article history:

Received 17 July 2017

Received in revised form 17 October 2017

Accepted 7 November 2017

Available online 8 November 2017

#### Keywords:

Plastic compression

Collagen scaffold

Tendon

Ligament

Annulus fibrosus

Tissue engineering

### ABSTRACT

We developed a new method to manufacture dense, aligned, and porous collagen scaffolds using biaxial plastic compression of type I collagen gels. Using a novel compression apparatus that constricts like an iris diaphragm, low density collagen gels were compressed to yield a permanently densified, highly aligned collagen material. Micro-porosity scaffolds were created using hydrophilic elastomer porogens that can be selectively removed following biaxial compression, with porosity modulated by using different porogen concentrations. The resulting scaffolds exhibit collagen densities that are similar to native connective tissues (~10% collagen by weight), pronounced collagen alignment across multiple length scales, and an interconnected network of pores, making them highly relevant for use in tissue culture, the study of physiologically relevant cell-matrix interactions, and tissue engineering applications. The scaffolds exhibited highly anisotropic material behavior, with the modulus of the scaffolds in the fiber direction over 100 times greater than the modulus in the transverse direction. Adipose-derived mesenchymal stem cells were seeded onto the biaxially compressed scaffolds with minimal cell death over seven days of culture, along with cell proliferation and migration into the pore spaces. This fabrication method provides new capabilities to manufacture structurally and mechanically relevant cytocompatible scaffolds that will enable more physiologically relevant cell culture studies. Further improvement of manufacturing techniques has the potential to produce engineered scaffolds for direct replacement of dense connective tissues such as meniscus and annulus fibrosus.

#### Statement of Significance

*In vitro* studies of cell-matrix interactions and the engineering of replacement materials for collagenous connective tissues require biocompatible scaffolds that replicate the high collagen density (15–25%/wt), aligned fibrillar organization, and anisotropic mechanical properties of native tissues. However, methods for creating scaffolds with these characteristics are currently lacking. We developed a new apparatus and method to create high density, aligned, and porous collagen scaffolds using a biaxial compression with porogens technique. These scaffolds have a highly directional structure and mechanical properties, with the tensile strength and modulus up to 100 times greater in the direction of alignment. We also demonstrated that the scaffolds are a suitable material for cell culture, promoting cell adhesion, viability, and an aligned cell morphology comparable to the cell morphology observed in native aligned tissues.

© 2017 Acta Materialia Inc. Published by Elsevier Ltd. All rights reserved.

### 1. Introduction

*In vitro* studies of cell-matrix interactions and the engineering of replacement materials for collagenous connective tissues

\* Corresponding author at: Department of Bioengineering, University of Utah, 36 S. Wasatch Drive, Rm. 3100, Salt Lake City UT 84112, United States.

E-mail address: [jeff.weiss@utah.edu](mailto:jeff.weiss@utah.edu) (J.A. Weiss).

<sup>1</sup> These authors contributed equally to this work.

require biocompatible scaffolds that replicate the high collagen density (15–25%/wt), aligned fibrillar organization, and anisotropic mechanical properties of native tissues. Collagen-based scaffolds, made from acid solubilized type I collagen, have been used extensively as 3D constructs for cell culture and tissue engineering [1–7]. Although these scaffolds are easy to fabricate and made of a natural material, they exhibit low density (0.1–0.5%/wt) and they are mechanically weak, rendering them unsuitable for most tissue

engineering applications. Alignment and densification of collagen gels has been achieved by mechanical deformation due to externally applied forces and/or cellular traction forces [8–13]. However, these efforts have generally fallen short of achieving the material density, alignment and material properties that are characteristic of highly aligned dense collagenous tissues such as ligaments, tendons, annulus fibrosus of the intervertebral disc, and meniscus. In contrast, decellularized tissues (e.g. intestinal porcine submucosa) have demonstrated a high level of success as an implantable scaffold for the repair of a variety of tissues [14–18]. However, decellularized tissues require a donor tissue and their density, shape and composition cannot be easily controlled, which limits their use for *in vitro* studies of cell–matrix interactions and tissue engineering applications. As such, there exists a clear need for methods to construct dense collagen scaffolds.

Within the last decade, several investigators have fabricated collagen scaffolds using uniaxial plastic compression of collagen gels [6,19–26]. In this method, low density collagen gels are subjected to uniaxial compression using a slow strain rate, forcing free water out of the matrix in the transverse plane and densifying the network of collagen fibrils [27]. The result is a thin, densified gel with collagen fibrils aligned in the transverse plane. This method has enabled construction of scaffolds with collagen density in excess of 20%/wt. Studies have utilized sheets of compressed collagen for the fabrication of tissue engineered dermis, cornea and muscle [23,24,28–32]. Rolled sheets of compressed collagen have been used to fabricate tissue engineered blood vessels [26], and some investigators have added microscale structural features to compressed collagen, such as grooves [33].

Although the plastic compression technique holds promise for tissue engineering applications, methods based on uniaxial compression impose a number of limitations. Compression along a single dimension results in a randomly aligned mat of collagen fibrils in the transverse plane. While this material symmetry may be a reasonable model of tissues such as dermis, it fails to replicate the aligned structure and organization present in many dense connective tissues such as tendon, ligament, meniscus, and intervertebral disc. The densification that occurs during plastic compression reduces porosity, which makes cell infiltration problematic [32]. Many studies have circumvented this problem by dispersing cells into the collagen gel prior to compression. However, in cases where this is not practical due to possible cell death during the manufacturing process, cell seeding will be limited to the surface of the compressed scaffold, and the density may impede cell infiltration during culture.

In this study, we developed a new method of biaxial plastic compression, yielding a densified collagen material with axially aligned transversely isotropic symmetry within the densified scaffold and controllable porosity. Porosity was created and controlled by introducing porogen particles into the collagen gel suspension prior to polymerization and compression. The resulting scaffolds demonstrated a significant longitudinal alignment of collagen fibrils and an interconnected network of pores. The scaffolds displayed distinct organizational motifs at different physical scales. Their organization was reminiscent of the organization in tendons and ligaments, which display a complex hierarchical organization of collagen, including nanometer scale fibrils, micrometer scale fibers, and mesoscale fascicles (or fiber bundles) (Fig. S1) [34,35]. Mechanical testing of the biaxially compressed scaffolds revealed that the stiffness in the direction of fibril alignment was over 100 times greater than the transverse direction, with a modulus nearly twice as large as reported for uniaxially compressed collagen gels [19]. Micro-CT imaging of thick scaffolds demonstrated that the porosity and transverse isotropy was maintained throughout the thickness of the scaffolds. Culture of adipose-derived mesenchymal stem cells (AD-MSCs) up to seven days resulted in minimal cell

death, demonstrating the cytocompatibility of the resulting scaffolds. Our method provides a new means of fabricating dense, aligned type I collagen scaffolds that will enable more physiologically relevant cell culture studies, while providing the basis for future development of mechanically relevant cytocompatible scaffolds for engineered dense connective tissues.

## 2. Materials and methods

### 2.1. Overview of manufacturing process

The manufacturing process consists of three distinct phases (Fig. 1). In the first phase, collagen gels are polymerized, either with or without porogens, in rectangular molds. This results in a low density network of collagen fibrils with interspersed porogens. In the second phase, the gels are compressed along two orthogonal directions, which drives out fluid in the direction perpendicular to the plane of compression (referred to herein as the longitudinal direction), densifies the hydrogel and aligns the collagen fibril network. The compression along two orthogonal directions causes fibrils to align in the longitudinal direction. At the end of this phase, the dense and aligned scaffolds have porogens interspersed within the collagen. In the third phase, the scaffolds are rinsed in an ethanol solution, which dissolves the porogens and leaves behind a porous network within the densified and aligned collagen fibril network.

### 2.2. Porogen manufacturing

Porogen microsphere aggregates were manufactured from a hydrophilic polyurethane elastomer (Hydromed Series D3, Advansource Biomaterials, Wilmington, MA, USA). This material absorbs water and at equilibrium it is ~50% water by weight, which reduces the specific gravity and prevents excessive settling. Since the material is hydrophilic, the particles evenly disperse, in contrast to hydrophobic microparticles that tend to aggregate in water. To manufacture the porogens, 3 g of elastomer was dissolved in 60 ml of 100% ethanol at 60 °C. The solution was stirred and maintained at 60 °C on a heated stir plate for 60 min and allowed to fully dissolve. While still warm, the solution was placed in a freezer at –20 °C for a minimum of three hours. This initiated a phase inversion, which created microsphere aggregates of the elastomer. After the elastomer microsphere aggregates had precipitated, the solution was agitated and then poured into 300 ml of chilled water (~5 °C) and further agitated. This diluted the ethanol solution and prevented the elastomer microsphere aggregates from re-dissolving in the solution. The microsphere aggregates were allowed to settle overnight and the remaining water was pipetted off, leaving a high density solution of microsphere aggregates. This solution was centrifuged for 30 s at 5000g and the excess water was decanted. The centrifuged aggregates were lyophilized, weighed and re-suspended in DI water at a concentration of 40 mg/ml to form a stock solution. Since the drying process caused the microsphere aggregates to partially fuse, a tissue homogenizer was used to break them up, forming aggregates with diameters ranging from 25 to 500 µm.

### 2.3. Collagen gel polymerization

Collagen gels were made from a 10 mg/ml stock solution of acid solubilized type I collagen, which was purified from rat tail tendons based on previously published protocols [36,37]. Briefly, tendons were isolated from freshly frozen Sprague-Dawley rat tails (BioreclamationIVT, Westbury, NY, USA) and cleaned by immersion in 70% isopropanol for 60 min. Clean tendons were placed in 0.02 N

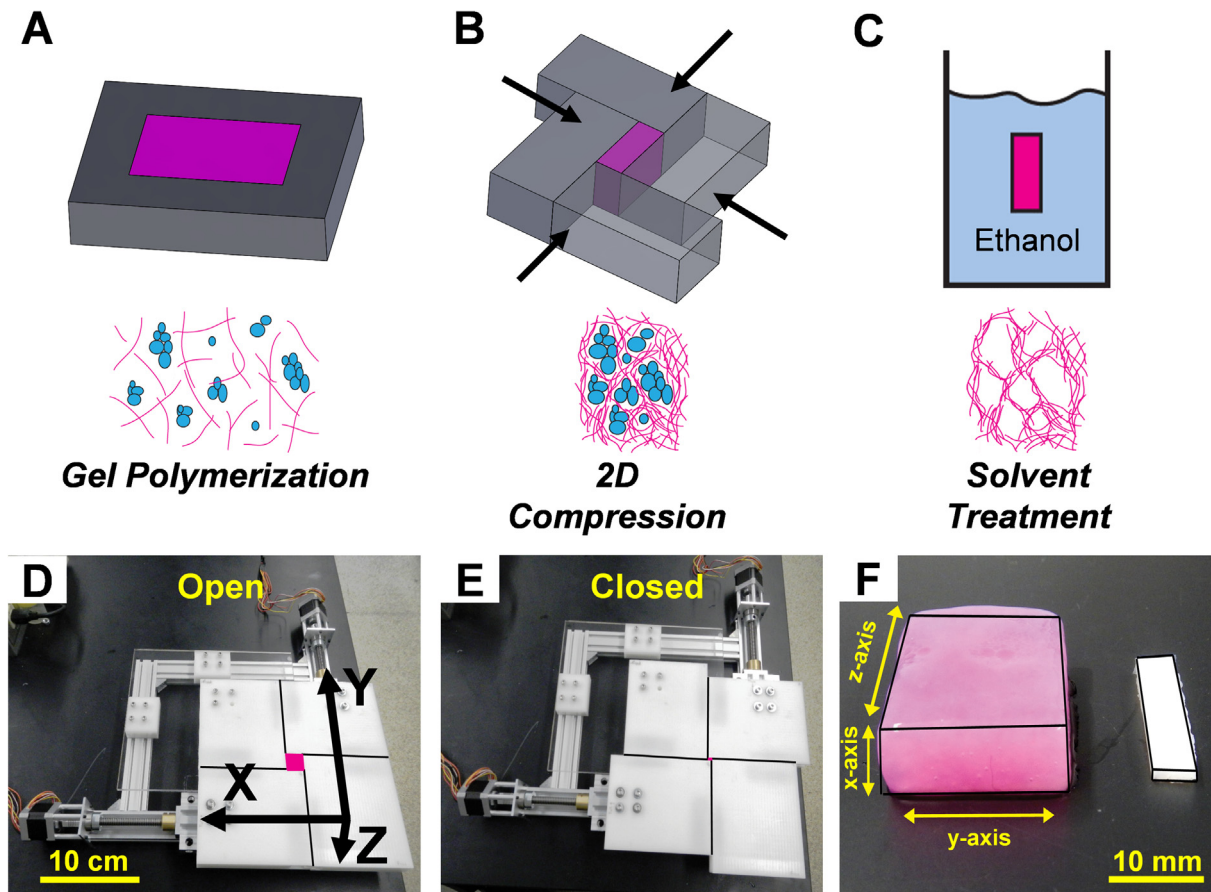


**Fig. 1.** Fabrication of biaxial compressed collagen scaffolds. The top row contains schematic processing steps and accompanying representation of the fibril network in the collagen gel. (A) An acid solubilized collagen solution (pink) containing suspended porogen particles (blue) was polymerized in a rectangular mold. (B) Polymerized collagen gels underwent biaxial plastic compression to densify the collagen network. (C) Compressed collagen gels were washed in ethanol to dissolve porogens, leaving a dense, porous collagen scaffold. (D) Biaxial compression device used for plastic compression of collagen gels in the open state. (E) Collagen gels were placed in the opening between the blocks and stepper motors drove the block faces together, laterally compressing the collagen gel. (F) The dimensions of the final compressed gel (white) had the same length, but greatly reduced width and thickness relative to the uncompressed gel (pink). Pink color of the uncompressed gel was due to phenol red in the polymerized collagen gels, which was washed out during the porogen removal process. Black outlines were added to help clarify shape and dimensions. (For interpretation of the references in this figure legend, the reader is referred to the web version of this article.)

acetic acid and stirred for 48–72 h at 4 °C to extract acid soluble collagen. Impurities were removed by ultra-centrifugation (30,000g for 45 min) and collection of the supernatant containing the acid soluble collagen. To achieve high concentration stock solutions, the collagen was isolated from the supernatant by precipitation with NaCl [36]. Under constant stirring, concentrated NaCl solution was added to the supernatant to a final concentration of 0.4 M NaCl and stirred for 60 min at 4 °C. Collagen precipitate was collected by immediate ultracentrifugation (30,000 g for 45 min) and collection of the collagen pellet. Collagen pellets were frozen at 20 °C, lyophilized, and dissolved in 0.02 N acetic acid at 10 mg/ml. The stock collagen solution was pipetted into a 50 ml centrifuge tube and a controlled amount of the porogen stock solution was added and gently mixed by rocking the tube back and forth. The amount of porogen stock solution depended on the desired concentration of porogen. After this, 10 × PBS with phenol red (as a pH indicator) was added such that a 1 × PBS concentration was obtained in the final solution. Deionized water was added to fill the remaining volume so that the final concentration of collagen was 6 mg/ml, which was the concentration used for all gels. Gels were then neutralized with an appropriate amount of 1 N NaOH to a pH of ~8. The solution was then poured into rectangular molds (25 mm × 40 mm × 6 mm) and allowed to polymerize overnight at room temperature in a covered container (Fig. 1A). Three

different groups of gels were created. A control group was polymerized with no porogens, while two other groups were polymerized with porogen concentrations of 6 mg/ml (a ratio of porogen to collagen of 1:1) and 12 mg/ml (a ratio of porogen to collagen of 2:1). All gels were the same volume and contained the same concentration of collagen. The porogen concentration and amount of water were altered to obtain the desired porogen concentration and to maintain the gel volume.

#### 2.4. Biaxial compression and porogen removal

Polymerized gels were placed in a custom made compression apparatus and serially compressed along two orthogonal directions (Fig. 1B). The compression apparatus consisted of four Delrin blocks (12.5 cm × 12.5 cm × 2.5 cm) that formed a jaw that closes and opens like an iris (Fig. 1D and E). Rectangular pockets were machined into the blocks to hold neodymium magnets. The strong magnets ensured that the block faces remained flush during actuation, maintaining the rectangular cross-section of the scaffold. Two linear actuators, driven by stepper motors, were used to open and close the jaws along two independent axes. The order of actuation and speed of the stepper motors were controlled by LabVIEW (National Instruments, Austin, TX, USA). Prior to compression, polymerized hexahedral gels were placed into the open jaws,

which were then moved until flush with all sides of the gel. Gels were first compressed along the y-axis at 0.5 mm/min until a compressive strain magnitude of 80% was reached. Following this, gels were then compressed along the x-axis at the same speed and to the same level of strain. For the collagen gels with starting dimensions of 6 mm × 40 mm × 25 mm, this resulted in scaffold dimensions under compression of 1.2 mm × 8 mm × 25 mm. After active compression along both directions, the jaws were held in place and the gels were allowed to equilibrate for 20 min at the compressed dimensions, after which the jaws were opened and the compressed scaffolds were removed (Fig. 1F). During compression, fluid exuded from the top and bottom of the gel surface. Scaffolds were then rinsed three times in 80% ethanol for 24 h, which removed the porogen material (Fig. 1C). During the rinses, gels were placed in closed flasks at 5 °C on a shaker plate. Prior to testing, imaging and cell seeding, gels were placed in 1X PBS and allowed to equilibrate overnight.

### 2.5. Imaging and image analysis of Acellular scaffolds

Acellular scaffolds were imaged using multiphoton microscopy, scanning electron microscopy (SEM) and micro-CT. For multiphoton imaging, scaffolds in PBS were placed between two cover slips that were separated by double stick tape (3M VHB, 1 mm thick) with a thickness similar to the scaffolds, which prevented compression. The samples were placed under the objective of an inverted multiphoton microscope (Ultima, Bruker Nano, Middleton, WI, USA). Scaffolds were imaged using an excitation wavelength of 855 nm, detecting collagen second harmonic generation (SHG) signal (435–485 nm filter band). A 16X objective was used for image acquisition. Multiple-field mosaics were assembled using the built-in software of the microscope and assembled using the Grid/Collection stitching plugin [38] within ImageJ (NIH, Bethesda, MD, USA). Images were acquired at depths ranging from the scaffold surface to 100 μm. Past this point, the signal was lost due to scattering effects within the dense collagen scaffold. Images of the collagen gels were also acquired prior to compression and porogen removal. The red channel (570–620 nm filter band) yielded the signal for the porogen material. Porosity of the compressed scaffolds was computed for each group by converting each image within a stack to a binary image using an automated thresholding algorithm, Otsu's method [39], available within ImageJ, then dividing the total number of black pixels (pore space) by the total number of pixels in the image. The mean and standard deviations for porosity were computed for all three porogen groups (n = 3 each group).

For SEM imaging, 2:1 porogen to collagen scaffolds were stained with osmium tetroxide and uranyl acetate and dehydrated with hexamethyldisilazane, sputter coated with a 5 nm layer of gold-palladium and imaged at 10 kV at magnifications ranging from 5× to 15000× (Quanta 600 FEG, FEI, Hillsboro, OR, USA). Fiber alignment within the SEM images was analyzed using a fast Fourier transform based fiber orientation algorithm [40]. This algorithm outputs a polar plot of fiber alignment vs. angle, as well as an anisotropy parameter, which ranges from 0 (perfectly random) to 1 (perfectly aligned). See Fig. S2 for an example of orientation plots and anisotropy values for a set of synthetic fiber images. Analysis was performed on images at magnifications of 50×, 1000× and 15000× to measure structural anisotropy at the millimeter, micrometer, and nanometer scales, respectively, using images from 5 locations at each magnification for analysis. Statistical analysis was conducted using t-tests with Holm-Sidak correction for multiple comparisons. For micro-CT imaging, a thick 2:1 porogen to collagen scaffold (3 mm thick vs. 1 mm thick for all other scaffolds) was manufactured and stained using osmium tetroxide and uranyl acetate. The sample was imaged in PBS using micro-CT (Inveon PET/CT, Siemens Medical Solutions, Malvern, PA, USA) with a voxel

size of 20 μm. Image data was imported into Amira (FEI, Hillsboro, OR, USA) where the orthoslice feature was used to qualitatively examine the 3D structure and organization of the scaffold. Additionally, slices were obtained from the center of the scaffold, both along the flat face and the face perpendicular to it. Beam hardening artifacts [41] made the outside of the scaffold appear brighter than the interior, and this was corrected by performing a background subtraction and local thresholding in ImageJ. This provided a binary image that revealed the pore and fiber structure through the volume of the thick scaffold.

### 2.6. Mechanical testing of scaffolds

Samples were subjected to constant strain rate uniaxial tensile testing. Test samples were obtained both along and transverse to the fiber direction, corresponding to the z and y axes, respectively (Fig. S3). Samples were frozen at –20 °C and then cut with a custom punch made from straight edge razor blades to produce a test specimen with straight edges. For longitudinal testing, scaffolds were cut along the z-axis into slices 3 mm wide (Supplementary Fig. 2A). For testing in the transverse direction, samples were cut into strips using the same punch, but along the y-axis (Supplementary Fig. 2B). Samples were then loaded into a custom tensile testing system consisting of a horizontal brushless servomotor driven linear actuator (Aerotech Inc., Pittsburgh, PA, USA), two machined aluminum clamps suspended in a PBS bath and a 8.9 N load cell [5,42]. Prior to testing, sample width and thickness were measured with digital calipers. After placing samples into the clamps, the reference length was measured and a tare load was applied (0.01 N for longitudinal samples and 0.002 N for transverse samples). Samples were strained in tension at a rate of 0.5% s<sup>-1</sup> grip-to-grip strain until failure. The testing and data acquisition was controlled using LabVIEW. At least 4 samples were tested from each group (2:1, 1:1, and control) for samples harvested along both the fiber and transverse directions. A subset of the samples exhibited clamp slippage and/or failed at the clamp interface. To ensure that the material properties calculated from the stress-strain curves most closely represented the true material behavior, samples that reached the highest stress at failure while showing no video or graphical evidence of clamp slippage were selected for analysis (at least 3 samples for each group). The tangent modulus of samples cut along the fiber direction was calculated between 12 and 15% strain, and the tangent modulus of samples cut transverse to the fiber direction was calculated between 50 and 75% strain. These ranges were selected because all samples in each group consistently experienced the chosen ranges of strain (no failures before maximum strain for the range). Tensile strength, ultimate strain, and tangent modulus of the experimental groups were compared to the control group using t-tests with Holm-Sidak correction for multiple comparisons. Additionally, the tensile strength, ultimate strain, and tangent modulus of the 2:1 group were compared to values from the literature for uniaxially compressed type-I collagen scaffolds [19] using t-tests with Holm-Sidak correction for multiple comparisons.

### 2.7. Cell culture and imaging of cell seeded scaffolds

Following porogen removal, 2:1 porogen to collagen compressed scaffolds were cut into 5 mm × 10 mm sections and sanitized in 80% ethanol for 24 h. Prior to cell seeding, scaffolds were placed in 12-well culture plates, rinsed in PBS for 24 h, followed by incubation in cell culture media overnight. Culture media was aspirated from each well and scaffolds were seeded on the top surface with 125,000 cells/scaffold (2,500 cells/cm<sup>2</sup>) of AD-MSCs (SCRC-4000, ATCC, Manassas, VA, USA), in MSC Basal Medium supplemented with the growth kit for AD-MSCs (PCS-500-030

and PCS-500-040, ATCC, Manassas, VA, USA) and 25  $\mu\text{g}/\text{mL}$  gentamicin (Thermo Fisher Scientific, Waltham, MA, USA). Scaffolds were incubated at 37 °C for 1 h before filling wells with media. Cell seeded constructs were cultured for 1, 3, or 7 days ( $N \geq 3$  scaffolds at each time point), exchanging media every 2–3 days. Cell viability was analyzed using calcein-AM/ethidium homodimer staining (Thermo Fisher Scientific, Waltham, MA, USA), where calcein-AM undergoes an esterase conversion to calcein in live cells, emitting green fluorescence, and ethidium homodimer penetrates the membrane of non-viable cells and emits red fluorescence upon DNA intercalation. Scaffolds were incubated in live/dead dyes (5  $\mu\text{M}$  calcein-AM and 5  $\mu\text{M}$  ethidium homodimer in PBS) for 40 min. at 37 °C, then rinsed in PBS and imaged by widefield fluorescence for live/dead analysis. Images were acquired in 3 locations along the width of the gel in each sample to provide a representative sampling across the entire gel. Images were analyzed to determine the percent live cells in each image, and the data for the three locations were averaged to obtain a single data point for each image. A one-way ANOVA was used to assess the effect of culture time on cell viability and post hoc comparisons were performed using Tukey's method.

Following viability imaging, scaffolds were fixed in 10% formalin for 24 h and then transferred to 70% ethanol. Fixed samples were imaged using multiphoton microscopy (Bruker Nano, Middleton, WI, USA) to localize cells on the collagen scaffold. Cells were imaged using 780 nm excitation, detecting two-photon excited fluorescence of calcein AM dye (500–550 nm filter band). Collagen was imaged at 855 nm laser and detecting the collagen SHG signal (435–485 nm filter band). At each location imaged, identical image frames were acquired (i.e. same x, y center and z-height) for both cell fluorescence and collagen SHG. Extended depth of field images were constructed using Adobe Photoshop (Adobe Systems, San Jose, CA, USA) and composites of extended depth of field images and z-stacks were created using ImageJ software (NIH, Bethesda, MD, USA). Volumetric images of multiphoton z-stacks were created using FluorRender software [43].

## 2.8. Statistical analysis

Statistical analysis was performed using the Stata 14 software (StataCorp, College Station, TX, USA), except for live/dead analysis which was performed using JMP software. All values are expressed as mean  $\pm$  standard deviation, except for mechanical testing data and material properties which are expressed as mean  $\pm$  standard error of the mean (s.e.m.). The significance tests used for statistical comparisons, and multiple comparison procedure as appropriate, are indicated in each methods section. Significance was established at the level  $\alpha = 0.05$  for all significance tests.

## 3. Results

### 3.1. Scaffold manufacturing and morphology

Optical transmission microscopy revealed that the hydrophilic polyurethane porogens were composed of microsphere aggregates, where individual microspheres were 25–75  $\mu\text{m}$  in diameter, and the aggregates ranged in size from 50 to 500  $\mu\text{m}$  (Fig. 2A). Multiphoton images of the top and bottom of the gels prior to compression revealed that the aggregates were evenly distributed throughout the gel (Fig. 2B). Images taken after gel compression, but before porogen removal, showed that the elastomer porogen particles were deformed along the direction of fiber alignment (Fig. 2C).

The final dimensions of the scaffolds were  $1.3 \pm 0.1$  mm in thickness,  $10.3 \pm 0.8$  mm in width, while the length remained unchanged (25 mm), so that the final scaffold volume was 5.6% of the initial volume of the collagen gel. These dimensions reflect

a slight swelling that occurred after samples were soaked in PBS after ethanol washing (scaffolds were initially compressed to 1.2 mm thickness and 8 mm width). With these initial and final dimensions, this represents a densification of nearly 18 times, resulting in a final collagen concentration of  $\sim 10\%$  by weight.

Mosaic multiphoton images revealed a significant difference in porosity between groups (Fig. 2D–F). The 2:1 porogen: collagen group were highly porous ( $37 \pm 7\%$ ), displaying an interconnected network of pores and connecting fiber structures. The 1:1 porogen: collagen group displayed less porosity ( $22 \pm 5\%$ ), but still had a large number of interconnected pores, but with thicker interconnecting fibers. The control group, with no porogen, displayed considerably less porosity than either group with porogens ( $6.3 \pm 6.4\%$ ). However, small pores were still visible. In all groups, the pores were elongated in the z-axis, as were the interconnecting fibers. Since multiphoton imaging can only penetrate  $\sim 100$   $\mu\text{m}$  from the surface of the sample, micro-CT imaging was performed in order to visualize the interior structure of the scaffolds. Qualitative analysis of the 3D micro-CT data set revealed a similar aligned, interconnected porous network that was evenly distributed over the interior of the biaxially compressed scaffold (Fig. 2G).

### 3.2. Multiscale scaffold alignment

SEM imaging revealed that collagen fiber structures as well as collagen fibrils were aligned with the scaffold z-axis, and the extent of alignment was a function of physical scale (Fig. 3). To measure the level of alignment, an anisotropy index was defined, where a value of 0 represents a totally random organization and a value of 1 represents a perfectly aligned organization [40]. At the mesoscale ( $\sim 200$   $\mu\text{m}$ –1 mm), fiber structures and pores were highly aligned, with an anisotropy index of  $0.77 \pm 0.13$ . At the micro scale (1  $\mu\text{m}$ –100  $\mu\text{m}$ ), there was alignment of wrinkles on the surface of the connecting fibers, but less organization, with an anisotropy index of  $0.56 \pm 0.08$ . At the nanoscale ( $< 1$   $\mu\text{m}$ ), there was clear alignment of collagen fibrils, but to a lesser extent, with an anisotropy index of  $0.39 \pm 0.13$ . Visual inspection of the image fields revealed higher collagen fibril alignment on the connecting fibers and lower alignment within the pores. The nanoscale anisotropy of uniaxially compressed collagen gels presented in the literature [19,28,30] was  $0.28 \pm 0.08$ , which is not significantly different from the nanoscale anisotropy of the biaxially compressed scaffolds in the present study ( $p = .24$ ).

### 3.3. Anisotropic material properties of scaffolds

The material properties of the scaffolds demonstrated that samples harvested along the longitudinal direction were substantially stiffer than those harvested along the transverse direction (Fig. 4, Fig. S4). The tensile strength and modulus of scaffolds tested along the longitudinal direction were 1 and 2 orders of magnitude larger than the transverse direction, respectively. The material properties of the 2:1 scaffolds were superior to those reported for uniaxially compressed type-I collagen scaffolds (Fig. 5). Tensile strength and modulus were significantly higher, while ultimate strain was significantly lower for the 2:1 scaffolds (modulus  $1.5 \pm 0.4$  MPa, tensile strength  $0.6 \pm 0.1$  MPa, and ultimate strain  $55 \pm 14\%$ ) [19,27]. Notably, the modulus of the 2:1 biaxially compressed scaffolds was nearly double the modulus reported for uniaxially compressed collagen ( $3.02 \pm 0.26$  vs.  $1.5 \pm 0.4$  MPa;  $p < .001$ ). With the exception of tensile strength ( $p = .001$  for 2:1 vs. control), there was no effect of the addition of porogens on the modulus, tensile strength, or failure strain ( $p = .91, .42$  and  $.76$  for modulus, tensile strength and failure strain for the 1:1 longitudinal tests;  $p = .13, .91$ , and  $.001$  for the 2:1 longitudinal tests;  $p = .91, .49$  and  $.12$  for the 1:1 transverse tests;  $p = .91, .99, .99$  for the 2:1 longitudinal tests).

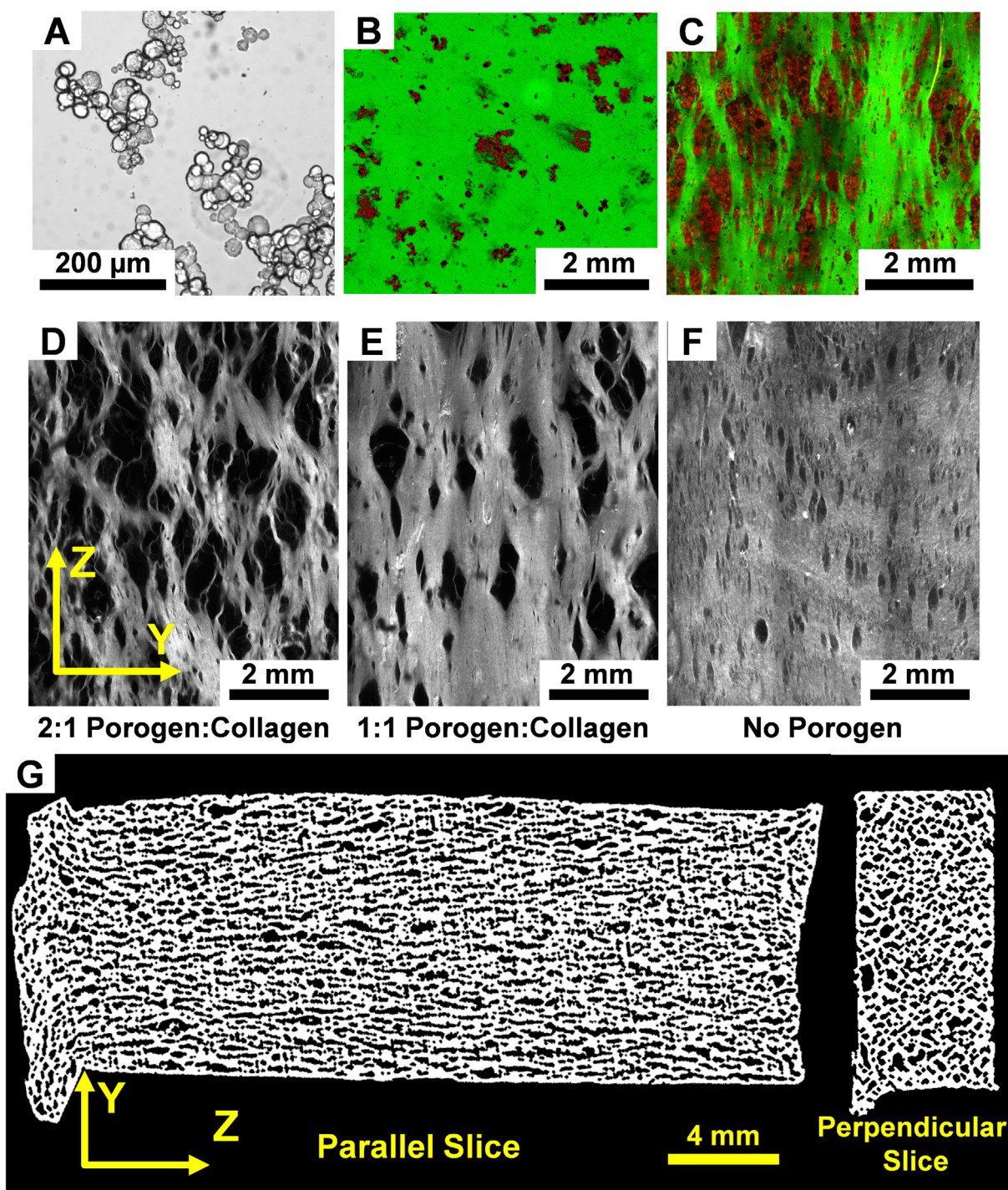


**Fig. 2.** (Top Row) Porogen morphology and distribution in collagen gels. (A) A 20X optical transmission microscope image of the porogen aggregates in water. (B) 4X multiphoton confocal microscopy image of a gel prior to compression showing even distribution of the porogen aggregates. Collagen SHG signal is shown in green and two photon excited fluorescence signal from the porogen signal in red. (C) 4X multiphoton confocal microscopy image after 2D compression, revealing that porogen aggregates compress and align in longitudinal direction. (Bottom Row) Effect of porogen content on microstructure. The ratio of porogen to collagen had a significant effect on the microstructural organization of the surrogates, where a high porogen content (D) resulted in substantially more porosity than lower porogen content (E) and no porogens (right). Longitudinal and transverse slices from micro-CT volumetric imaging of a 2:1 sample show a highly aligned fiber and connected pore structure in the center of the thick sample. The transverse slice shows similar pore structure, but does not demonstrate alignment. Axes depicted in panel D apply to all panels A-F, with the z and y-axes corresponding to the longitudinal and transverse material axes, respectively.

### 3.4. Cell culture on scaffolds

Cell seeded scaffolds contained viable, adhered cells at all time points, indicating that the scaffolds provided an excellent substrate for cell adhesion, cell growth, and cell proliferation (Fig. 6). The

scaffolds contained  $98.0 \pm 0.7$ ,  $93.9 \pm 2.7$ , and  $88.6 \pm 12.6$  percent live cells at 1, 3, and 7 days, respectively, as counted from live/dead staining fluorescence images (Fig. 6A–C). There was no significant difference in cell viability between any of the time points (day 1 vs. 3,  $p = .73$ ; day 1 vs. 7,  $p = .31$ ; day 3 vs. 7,  $p = .68$ ). Both

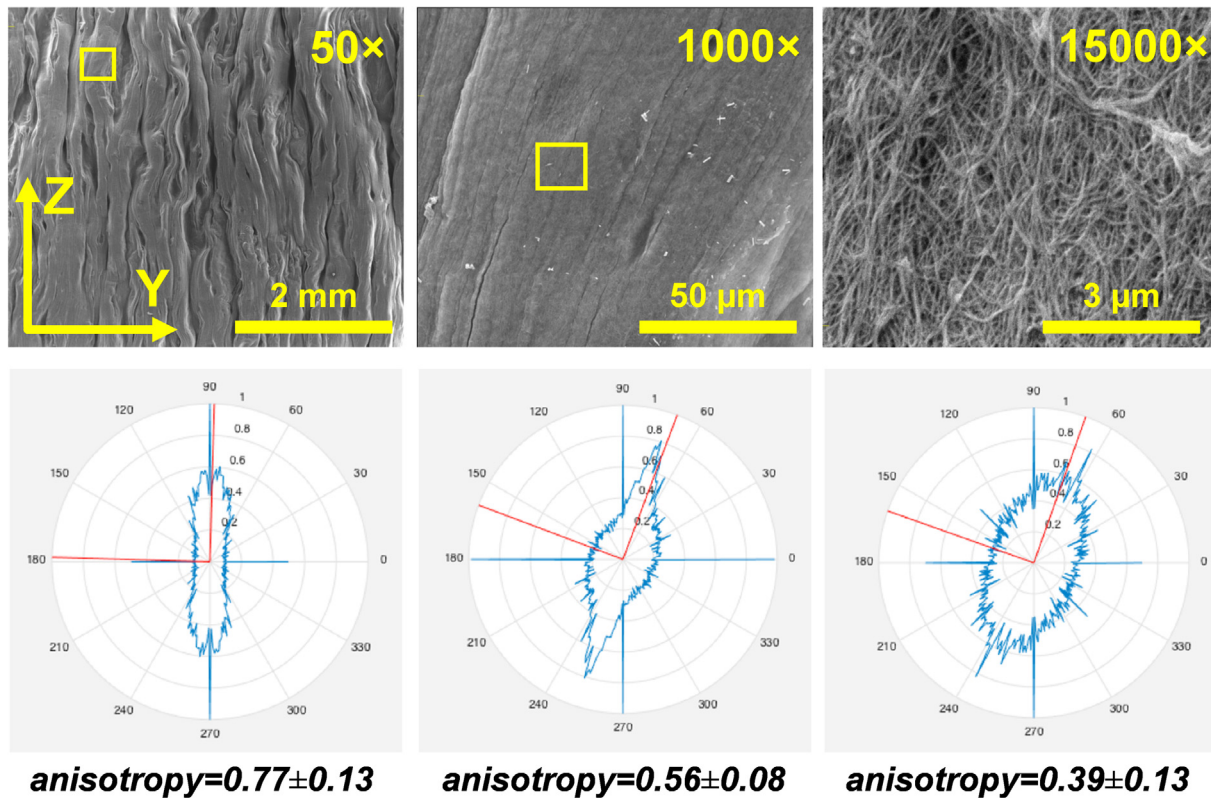


**Fig. 3.** Multiscale anisotropy of 2:1 porogen to collagen, biaxially compressed collagen scaffolds. Top row shows SEM images at the magnification specified in top right corner. Bottom row shows corresponding polar plot from the image analysis, where the red lines represent the primary fiber axis and the blue line is the magnitude of alignment at the specified angle. Note that some images were acquired at an angle. (Left Column) A 50 × SEM image shows highly aligned collagen fiber bundles and pores at the meso scale, which is reflected in the tight distribution of the plot of fiber orientation shown below and high anisotropy value. (Middle Column) 1000 × SEM image (taken from within the yellow box in the 50 × image) shows aligned ridges and folds at the micro scale, with a lower anisotropy than the meso scale, as reflected in the fiber orientation plot. (Right Column) 15000 × SEM image (taken from within the yellow box in the 1000 × image) shows that fibrils are aligned at the nano scale, but less than the larger scale levels, which is reflected in wider angle distribution in the fiber orientation polar plot. Anisotropy is reported as mean ± std from N = 6 images at each magnification.

widefield and multiphoton fluorescence microscopy revealed that cells resided on the surface and in the engineered open pore structure of the scaffolds. Notably, by day 7 cells had started to congregate in pores and along ridges on the scaffold surface (Fig. 6E and G). Most cells had an aligned, spindle shaped morphology throughout the 7-day experiment. However, in regions of especially high cell density and at the inside of some pore structures, cells had a more rounded appearance. Multiphoton microscopy enabled localization of the adhered cells within the collagen scaffold, revealing that the cells adhered to the collagen fibers and within the pore space, aligning to the local fiber axis. Volumetric images constructed from multiphoton z-stacks showed cells penetrating the scaffold via the interconnected pore network as early as day 1 and by days 3 and 7 cells had penetrated the entire imaging depth in some locations (Fig. 6F and G).

#### 4. Discussion

This research developed a novel apparatus and method to generate physiologically relevant collagen scaffolds that exhibit collagen density, fibril alignment and material properties that are representative of some dense connective tissues. Whereas scaffolds generated by uniaxial plastic compression exhibit an isotropic microstructure within the plane of compression, biaxially compressed scaffolds have a highly aligned microstructure along a single axis at the millimeter scale. The structural anisotropy and multiscale organization are hallmark features of aligned connective tissues such as tendon, ligament, annulus fibrosus, and

meniscus. The anisotropic organization of collagen fibrils within these tissues is vital in providing the mechanical strength necessary to bear high musculoskeletal loads. Mechanical testing of the scaffolds revealed significant anisotropy in the material properties as well, indicating that the scaffolds are capable of reproducing this important characteristic of dense connective tissues. Analysis of structural anisotropy in the SEM images revealed different organizational motifs at different physical scales. At the meso-scale, large bundles of collagen fibrils had an organization and size similar to collagen fascicles within tendon and ligament [34,35]. At the microscale, wrinkles of collagen fibrils had a similar size and orientation to collagen fibers within aligned connective tissues such as tendon, while at the nanoscale collagen fibrils had preferential alignment also seen in these tissues. Cells cultured on the scaffolds aligned themselves with these morphological features, indicating that not only are the scaffolds non-cytotoxic, but that they also stimulate cell adhesion and provide contact guidance cues for alignment. Given the importance of hierarchical organization in normal tissue function, recapitulating such features will be useful for *in vitro* studies and engineering of these tissues.

Biaxially compressed type-I collagen scaffolds provide a promising new engineered biomaterial for cell culture studies and tissue engineering, expanding on the 1D collagen compression technique developed by Brown et al. [27] while producing scaffolds with superior material properties and collagen architecture that is reminiscent of aligned dense connective tissues. While uniaxially compressed collagen gels have demonstrated encouraging results for use in many tissue engineering applications [21,23,24,26,28–32,44], they do not contain the multiscale alignment and high level

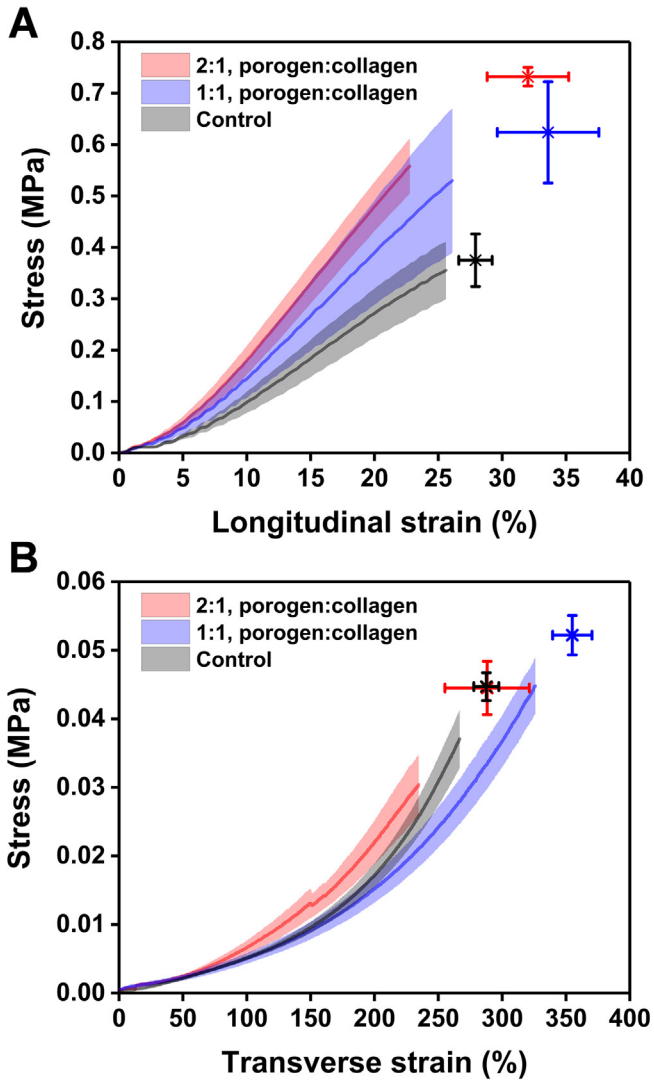


**Fig. 4.** Material properties of biaxially compressed collagen scaffolds. (A) Stress-strain curves for scaffolds tested along the longitudinal (fiber) direction. (B) Stress-strain curves for scaffolds tested transverse to the fiber direction. Note the significant differences in the scale of both axes between plots. The maximum stress for samples tested along the axial direction was over 100 times larger than for the transverse samples, and the axial samples were ten times less compliant. The longitudinal failure stress of 2:1 samples was significantly different from the control scaffolds, while failure stress, failure strain, and modulus were not significantly different from control for any of the other sample groups. Mean  $\pm$  s.e.m.

of mechanical anisotropy produced by biaxial compression [19,27]. Notably, while the biaxial compression with porogens technique produces mechanical anisotropy and significantly increased tensile strength and modulus compared to uniaxial compression, there was not a significant increase in anisotropy at the nanoscale for the biaxially compressed scaffolds. This unexpected lack of a difference at the nanoscale may be due to spatial variation in the alignment of collagen fibrils between the “fiber” and “pore” regions of the biaxially compressed scaffolds. Alternatively, it may indicate that more sensitive methods are required to characterize anisotropy at the physical scale of the collagen fibrils. Electrospinning is currently the most common technique to create highly aligned fibrous biomaterial scaffolds. Although electrospinning can produce scaffolds with varying fiber diameters [45,46], constituent components (i.e. two and three families of polymer fibers) [47], and level of alignment [46], it does not recreate the self-

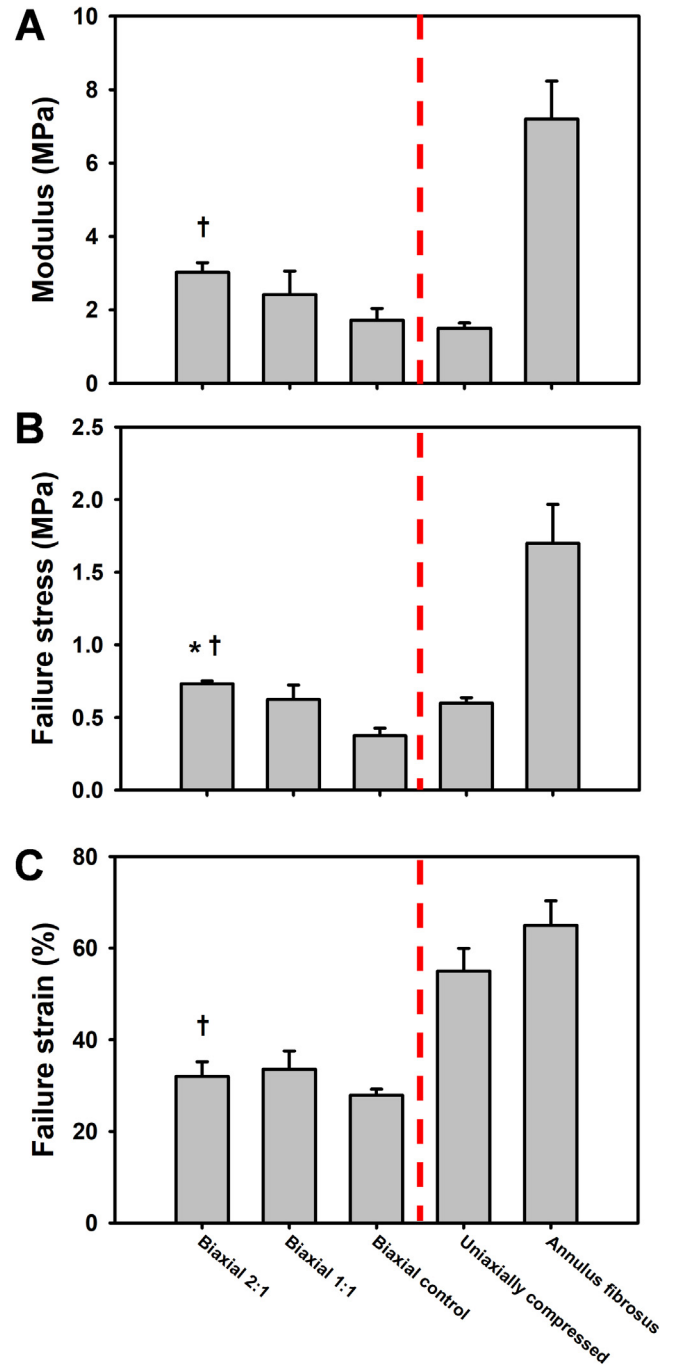


**Fig. 5.** Comparison of longitudinal material properties of biaxially compressed collagen scaffolds to uniaxially compressed collagen [19]. Tensile modulus (A), failure stress (B), and failure strain (C). The current 2:1 biaxially compressed scaffolds represent an improvement in modulus and failure strength compared to previous uniaxially compressed collagen. Data for the material properties of human annulus fibrosus are included for comparison [52]. Of the groups shown, the material properties of the 2:1 biaxially compressed collagen scaffolds compare the most favorably. Mean  $\pm$  s.e.m. \* indicates  $p < .05$  for comparison of biaxial samples to the biaxial control. † indicates  $p < .05$  for comparison of biaxial 2:1 and uniaxially compressed scaffolds.

assembled collagen fibrillar network [48]. Like electrospun scaffolds, our biaxial compression technique allows for high levels of porosity using porogens. To our knowledge, this is the first technique to produce an anisotropic natural biomaterial that reaches the mechanical properties of synthetic electrospun biomaterials such as polycaprolactone [49,50].

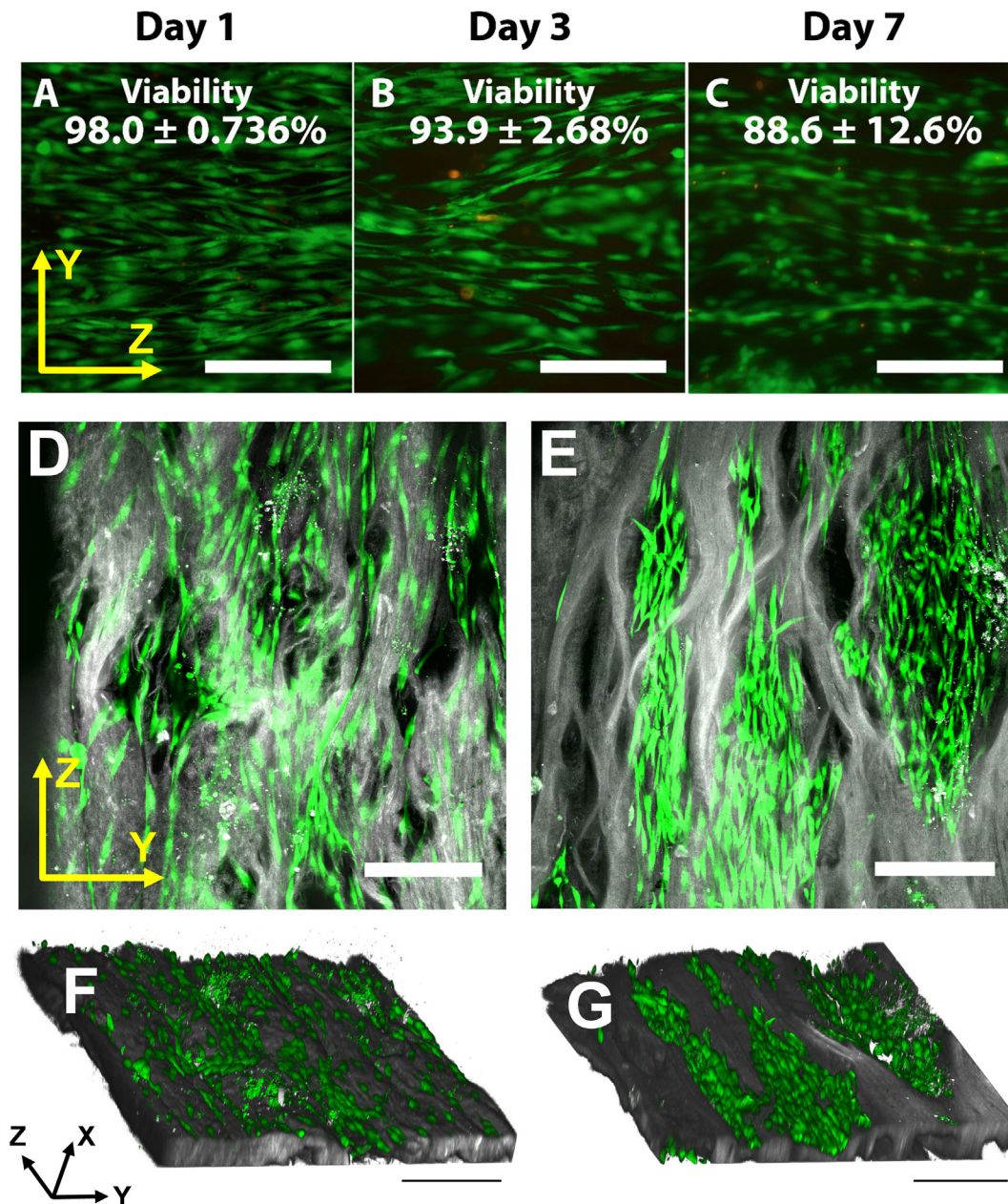


**Fig. 6.** Microscopy of adipose derived mesenchymal stem cell seeded scaffolds. Imaging of cell-seeded scaffolds over one week demonstrated cell viability and alignment of cells in the direction of collagen alignment. (A–C) Representative epi-fluorescence LIVE/DEAD<sup>®</sup> assay imaging cell viability (live (green):dead (red)) of cell seeded scaffolds at day (A) 1, (B) 3, and (C) 7 ( $n = 3–4$ ; mean  $\pm$  stdev). Multiphoton fluorescence microscopy images demonstrated cell infiltration and growth while revealing cell morphology in the context of scaffold architecture. (Top Row) At Days 1 (D) and 7 (E), extended depth of field images show that the cells (green) were adhered to the collagen scaffold surface (gray), while their spindle shaped geometry indicates that they began aligning with the scaffold fibers. (Bottom Row) Volume rendered z-stacks at Day 1 (F) and Day 7 (G) show that the cells have penetrated into the open pore structure of the scaffolds. All scale bars, 200  $\mu\text{m}$ . (For interpretation of the references to colour in this figure legend, the reader is referred to the web version of this article.)

The biaxial compression and porogen technique is a significant advancement for producing high density, aligned, natural biomaterial scaffolds; however the resultant mechanical properties are still below those of most native dense, aligned connective tissues (Fig. 5). It is often stated that it is desirable that the material properties of engineered scaffolds for tissue repair should match those of the target tissue, but it is not clear that achieving this goal is necessary for functional tissue regeneration and/or repair. Considering the natural processes of development and regeneration, it is possible that a scaffold with sufficient properties to withstand the mechanical and biological environment of implantation and early remodeling may provide sufficient structural and mechanical cues

for cell mediated regeneration (*in vitro* or *in vivo*) leading to improved functional outcomes and a more achievable engineering design target. A shift in thinking about scaffold design goals is evident within the field, as the focus moves toward the role of the scaffold in directing cellular behavior to recapitulate the healthy tissue environment rather than to directly replace the damaged tissue [51]. Currently, the biaxial compression technique produces collagen scaffolds with mechanical properties approaching that of the annulus fibrosus of the human intervertebral disc [52], making the scaffolds a promising starting point for a surrogate construct to represent the annulus fibrosus in cell culture studies or for tissue engineering efforts.

While this study investigated a range of manufacturing parameters, there are some limitations to the biaxial compression technique and differences between biaxially compressed scaffolds and native tissue. Although the scaffolds do exhibit some level of structural hierarchy across length scales (Figs. 2 and 3), they do not replicate native tissue hierarchy. Additionally, there are technical limitations associated with our current biaxial compression device. At present, our device can only manufacture rectangular materials that can be cut to the size and geometry required by an application. Although the maximum scaffold size we can currently manufacture while maintaining the same 80% compression along each axis is approximately 25 mm × 11 mm × 11 mm, this is only a limitation of the current apparatus and the biaxial compression technique is only limited in principle by the amount of materials available (collagen and porogens) and size of the compression apparatus. As presented here, our current method produces scaffolds ~10% collagen by weight, while uniaxial compression has been used to produce scaffolds up to 20% by weight. The increased collagen content reported for uniaxial compression is the result of increased magnitude of compression (>99% volume reduction vs. 94% volume reduction) and the use of additional techniques such as wicking away fluid [27] and applying multiple compressions [19]. Many of the techniques used to increase the collagen concentration for uniaxial compression could be adapted for use with our biaxial compression method.

Despite these limitations, there is great promise for the biaxial compression method, as additional techniques can be used to manufacture scaffolds with an even wider array of physiologically relevant material and physical properties. If scaffolds with increased modulus and tensile strength are desired, the initial collagen concentration can be increased along with the amount of biaxial compression. Our preliminary experiments suggest that achieving aligned scaffolds with up to 30% collagen/wet weight may be possible, which is approaching the concentration of native aligned connective tissues such as tendon and ligament [53–56]. Furthermore, crosslinking can be performed on the scaffolds, which will further increase their tensile strength and modulus [57–59]. The relative amount of compression along each axis can be varied, creating intermediate material symmetry and mechanical behavior. Porosity can be increased beyond the presented results simply by adding more porogens or increasing the porogen to collagen ratio, while the pore size and shape may be modified by using larger or smaller porogens. When increasing the porogen to collagen ratio, it would be important to consider that too much porogen could make the collagen too sparse and compromise the material's ability to function as a scaffold. However, while maintaining the same initial collagen concentration, gel volume, and magnitude of compression used for this study, we expect that the maximum achievable porogen concentration would not be great enough to compromise scaffold integrity. Additional surface morphologies, such as a crimp pattern similar to that observed at the fiber level of native tissues, can also be generated using multistage compression and a patterned compression surface [27,33,60]. Varying these parameters will facilitate the manufacture of tailored scaffolds for cell culture studies, and provide the ability to engineer tissue-specific scaffolds.

Although increased collagen density will produce scaffolds with increased tensile strength and modulus, cell penetration during culture is greatly reduced in higher density/lower porosity scaffolds [61,62]. By producing an interconnected network of pores in our scaffolds, seeded cells were able to penetrate through the pore structure. Because the pores form an interconnected network within the entire scaffold as evidenced by the micro CT images, it will be possible for cells to penetrate the entire depth of the scaffolds during extended culture. Flow mediated cell seeding methods may further facilitate the penetration of cells [63–66]. An addi-

tional benefit of an open pore structure is enhanced nutrient diffusion, which can be difficult to achieve in dense tissue scaffolds [6,67,68]. The addition of porogens resulted in an increase in modulus of the scaffolds. Although the increase was not statistically significant, the modulus of the 2:1 scaffolds was nearly twice that of the control biaxially compressed scaffolds. This increase in modulus may be explained by densification of collagen in the porogen-containing scaffolds. Since the same amount of collagen was used for all groups, the addition of porogens resulted in a higher density of collagen in the solid volume fraction of the scaffold, which may suggest that further increasing the porogen to collagen ratio may continue to increase collagen densification.

An important result of this study was the high level of cytocompatibility of the scaffolds, as demonstrated by live/dead staining of the cultured MSCs at 1, 3 and 7 days. Even at early time points, cells took on a spindle shape and were seen to align with the direction of fiber alignment. 3D imaging via multiphoton microscopy revealed that cells began forming an interconnected network within the connected pore network. Although this study focused on pure type I collagen as the scaffold material, additional proteins and molecules (e.g. glycosaminoglycans or proteoglycans) may be added, which may better emulate native tissues.

## 5. Conclusions

We developed an apparatus and method based on biaxial plastic compression of collagen gels that enabled the creation of high density collagen scaffolds with aligned collagen fibrils. Optical and electron microscopy revealed that aligned collagen structures spanned multiple physical scales, while material testing verified a strong level of mechanical anisotropy. Hydrophilic elastomer porogens were used to create an interconnected network of pores that aided in penetration of cells through the dense scaffold. MSCs cultured to 7 days revealed aligned, attached cells with minimal cell death, indicating that the resulting scaffolds were highly cytocompatible. Such scaffolds and manufacturing methods will prove highly relevant as a model system for studying cellular processes *in vitro* and for tissue engineering applications related to dense connective tissues such as annulus fibrosus, and future enhancements to the manufacturing methods may allow their material properties to be tailored to match dense connective tissues such as ligament, tendon and meniscus.

## Acknowledgments

We acknowledge financial support from NIH #R01AR047369 and R01EB015133. Imaging was performed at the Fluorescence Microscopy Core Facility, a part of the Health Sciences Cores at the University of Utah. Microscopes used in this research were obtained as part of a NCCR Shared Equipment Grant #1S10RR024761-01.

## Appendix A. Supplementary data

Supplementary data associated with this article can be found, in the online version, at <https://doi.org/10.1016/j.actbio.2017.11.017>.

## References

- [1] S.L. Schor, A.M. Schor, G.W. Bazill, The effects of fibronectin on the adhesion and migration of chinese hamster ovary cells on collagen substrata, *J. Cell Sci.* 49 (1981) 299–310.
- [2] B. Chevallay, D. Herbage, Collagen-based biomaterials as 3D scaffold for cell cultures: applications for tissue engineering and gene therapy, *Med. Biol. Eng. Comput.* 38 (2000) 211–218.
- [3] E. Cukierman, R. Pankov, D.R. Stevens, K.M. Yamada, Taking cell-matrix adhesions to the third dimension, *Science* 294 (2001) 1708–1712.

- [4] S. Rhee, F. Grinnell, Fibroblast mechanics in 3D collagen matrices, *Adv. Drug Deliv. Rev.* 59 (2007) 1299–1305.
- [5] S.P. Reese, B.J. Ellis, J.A. Weiss, Micromechanical model of a surrogate for collagenous soft tissues: development, validation and analysis of mesoscale size effects, *Biomech. Model. Mechanobiol.* 12 (2013) 1195–1204.
- [6] R.A. Brown, In the beginning there were soft collagen-cell gels: towards better 3D connective tissue models?, *Exp Cell Res.* 319 (2013) 2460–2469.
- [7] B.N. Mason, A. Starchenko, R.M. Williams, L.J. Bonassar, C.A. Reinhart-King, Tuning three-dimensional collagen matrix stiffness independently of collagen concentration modulates endothelial cell behavior, *Acta Biomater.* 9 (2013) 4635–4644.
- [8] V.H. Barocas, T.S. Girton, R.T. Tranquillo, Engineered alignment in media equivalents: magnetic prealignment and mandrel compaction, *J. Biomech. Eng.* 120 (1998) 660–666.
- [9] K.D. Costa, E.J. Lee, J.W. Holmes, Creating alignment and anisotropy in engineered heart tissue: role of boundary conditions in a model three-dimensional culture system, *Tissue Eng.* 9 (2003) 567–577.
- [10] R.D. Bowles, R.M. Williams, W.R. Zipfel, L.J. Bonassar, Self-assembly of aligned tissue-engineered annulus fibrosus and intervertebral disc composite via collagen gel contraction, *Tissue Eng. Part A* 16 (2010) 1339–1348.
- [11] N.K. Weidenhamer, R.T. Tranquillo, Influence of cyclic mechanical stretch and tissue constraints on cellular and collagen alignment in fibroblast-derived cell sheets, *Tissue Eng. C Meth.* 19 (2013) 386–395.
- [12] U.N. Wudebwe, A. Bannerman, P. Goldberg-Oppeneimer, J.Z. Paxton, R.L. Williams, L.M. Grover, Exploiting cell-mediated contraction and adhesion to structure tissues in vitro, *Philos. Trans. R. Soc. Lond. B Biol. Sci.* 370 (2015) 20140200.
- [13] J.L. Puetzer, E. Koo, L.J. Bonassar, Induction of fiber alignment and mechanical anisotropy in tissue engineered menisci with mechanical anchoring, *J. Biomech.* 48 (2015) 1436–1443.
- [14] S. Aiken, S. Badylak, J. Toombs, K. Shelbourne, M. Hiles, G. Lantz, D. Van Sickle, Small intestinal submucosa as an intra-articular ligamentous graft material: a pilot study in dogs, *VCOT Archive* 7 (1994) 36–40.
- [15] E. Hesse, G. Kluge, A. Atfi, D. Correa, C. Haasper, G. Berding, H.O. Shin, J. Vierung, F. Langer, P.M. Vogt, C. Krettek, M. Jagodzinski, Repair of a segmental long bone defect in human by implantation of a novel multiple disc graft, *Bone* 46 (2010) 1457–1463.
- [16] F.G. Scholl, M.M. Boucek, K.C. Chan, L. Valdes-Cruz, R. Perryman, Preliminary experience with cardiac reconstruction using decellularized porcine extracellular matrix scaffold: human applications in congenital heart disease, *World J. Pediatr. Congenit. Heart Surg.* 1 (2010) 132–136.
- [17] Y.Y. Gong, J.X. Xue, W.J. Zhang, G.D. Zhou, W. Liu, Y. Cao, A sandwich model for engineering cartilage with acellular cartilage sheets and chondrocytes, *Biomaterials* 32 (2011) 2265–2273.
- [18] C.W. Cheng, L.D. Solorio, E. Alsberg, Decellularized tissue and cell-derived extracellular matrices as scaffolds for orthopaedic tissue engineering, *Biotechnol. Adv.* 32 (2014) 462–484.
- [19] E.A. Abu Neel, U. Cheema, J.C. Knowles, R.A. Brown, S.N. Nazhat, Use of multiple unconfined compression for control of collagen gel scaffold density and mechanical properties, *Soft Matter* 2 (2006) 986–992.
- [20] T. Alekseeva, E. Hadjipanayi, E.A. Abu Neel, R.A. Brown, Engineering stable topography in dense bio-mimetic 3D collagen scaffolds, *Eur. Cells Mater.* 23 (2012) 28–40.
- [21] J.L. Bron, H.W. Mulder, L.A. Vonk, B.Z. Doulabi, M.J. Oudhoff, T.H. Smit, Migration of intervertebral disc cells into dense collagen scaffolds intended for functional replacement, *J. Mater. Sci. - Mater. Med.* 23 (2012) 813–821.
- [22] U. Cheema, R.A. Brown, Rapid fabrication of living tissue models by collagen plastic compression: understanding three-dimensional cell matrix repair, *Adv. Wound Care* 2 (2013) 176–184.
- [23] H.J. Levis, R.A. Brown, J.T. Daniels, Plastic compressed collagen as a biomimetic substrate for human limbal epithelial cell culture, *Biomaterials* 31 (2010) 7726–7737.
- [24] S. Mi, C.J. Connon, The formation of a tissue-engineered cornea using plastically compressed collagen scaffolds and limbal stem cells, *Meth. Mol. Biol.* 1014 (2013) 143–155.
- [25] P. Sawadkar, S. Alexander, M. Tolk, J. Wong, D. McGrouther, L. Bozec, V. Mudera, Development of a surgically optimized graft insertion suture technique to accommodate a tissue-engineered tendon in vivo, *Biores. Open Access* 2 (2013) 327–335.
- [26] H.Y. Tuan-Mu, P.C. Lu, P.Y. Lee, C.C. Lin, C.J. Chen, L.L. Huang, J.H. Lin, J.J. Hu, Rapid fabrication of a cell-seeded collagen gel-based tubular construct that withstands arterial pressure: rapid fabrication of a gel-based media equivalent, *Ann. Biomed. Eng.* 44 (2016) 3384–3397.
- [27] R.A. Brown, M. Wiseman, C.B. Chuo, U. Cheema, S.N. Nazhat, Ultrarapid engineering of biomimetic materials and tissues: fabrication of nano- and microstructures by plastic compression, *Adv. Funct. Mater.* 15 (2005) 1762–1770.
- [28] E. Braziliulis, M. Diezi, T. Biedermann, L. Pontiggia, M. Schmucki, F. Hartmann-Fritsch, J. Luginbuhl, C. Schiestl, M. Meuli, E. Reichmann, Modified plastic compression of collagen hydrogels provides an ideal matrix for clinically applicable skin substitutes, *Tissue Eng. C Meth.* 18 (2012) 464–474.
- [29] K. Hu, H. Shi, J. Zhu, D. Deng, G. Zhou, W. Zhang, Y. Cao, W. Liu, Compressed collagen gel as the scaffold for skin engineering, *Biomed. Microdevices* 12 (2010) 627–635.
- [30] S. Mi, B. Chen, B. Wright, C.J. Connon, Plastic compression of a collagen gel forms a much improved scaffold for ocular surface tissue engineering over conventional collagen gels, *J. Biomed. Mater. Res. A* 95 (2010) 447–453.
- [31] E.M. Engelhardt, E. Stegberg, R.A. Brown, J.A. Hubbell, F.M. Wurm, M. Adam, P. Frey, Compressed collagen gel: a novel scaffold for human bladder cells, *J. Tissue Eng. Regen. Med.* 4 (2010) 123–130.
- [32] H. Kayhanian, S. Jones, J. Phillips, M. Lewis, R. Brown, V. Mudera, Host muscle cell infiltration in cell-seeded plastic compressed collagen constructs, *J. Tissue Eng. Regen. Med.* 3 (2009) 72–75.
- [33] A. Kureshi, U. Cheema, T. Alekseeva, A. Cambrey, R. Brown, Alignment hierarchies: engineering architecture from the nanometre to the micrometre scale, *J. Royal Soc. Interface* 7 (Suppl 6) (2010) S707–S716.
- [34] J. Kastelic, A. Galeski, E. Baer, The multicomposite structure of tendon, *Connect. Tissue Res.* 6 (1978) 11–23.
- [35] K.D. Danylchuk, J.B. Finlay, J.P. Krcek, Microstructural organization of human and bovine cruciate ligaments, *Clin. Orthop. Relat. Res.* (1978) 294–298.
- [36] G. Chandrakasan, D.A. Torchia, K.A. Piez, Preparation of intact monomeric collagen from rat tail tendon and skin and the structure of the nonhelical ends in solution, *J. Biol. Chem.* 251 (1976) 6062–6067.
- [37] N. Rajan, J. Habermehl, M.-F. Cote, C.J. Doillon, D. Mantovani, Preparation of ready-to-use, storable and reconstituted type I collagen from rat tail tendon for tissue engineering applications, *Nat. Protocols* 1 (2007) 2753–2758.
- [38] S. Preibisch, S. Saalfeld, P. Tomancak, Globally optimal stitching of tiled 3D microscopic image acquisitions, *Bioinformatics* 25 (2009) 1463–1465.
- [39] N. Otsu, A threshold selection method from gray-level histograms, *IEEE Trans. Syst. Man Cyber.* 9 (1979) 62–66.
- [40] L. Krishnan, C.J. Underwood, S. Maas, B.J. Ellis, T.C. Kode, J.B. Hoying, J.A. Weiss, Effect of mechanical boundary conditions on orientation of angiogenic microvessels, *Cardiovasc. Res.* 78 (2008) 324–332.
- [41] R.A. Brooks, G. Di Chiro, Beam hardening in x-ray reconstructive tomography, *Phys. Med. Biol.* 21 (1976) 390–398.
- [42] S.P. Reese, C.J. Underwood, J.A. Weiss, Effects of decorin proteoglycan on fibrillogenesis, ultrastructure, and mechanics of type I collagen gels, *Matrix Biol.* 32 (2013) 414–423.
- [43] Y. Wan, H. Otsuna, C.B. Chien, C. Hansen, FluorRender: an application of 2D image space methods for 3D and 4D confocal microscopy data visualization in neurobiology research, *IEEE Pac. Vis. Symp.* (2012) 201–208.
- [44] T. Alekseeva, R.E. Unger, C. Brochhausen, R.A. Brown, J.C. Kirkpatrick, Engineering a microvascular capillary bed in a tissue-like collagen construct, *Tissue Eng. Part A* 20 (2014) 2656–2665.
- [45] J. Doshi, D.H. Reneker, Electrospinning process and applications of electrospun fibers, *J. Electrostat.* 35 (1995) 151–160.
- [46] C.A. Bashur, L.A. Dahlgren, A.S. Goldstein, Effect of fiber diameter and orientation on fibroblast morphology and proliferation on electrospun poly (D, L-lactic-co-glycolic acid) meshes, *Biomaterials* 27 (2006) 5681–5688.
- [47] B.M. Baker, A.O. Gee, R.B. Metter, A.S. Nathan, R.A. Marklein, J.A. Burdick, R.L. Mauck, The potential to improve cell infiltration in composite fiber-aligned electrospun scaffolds by the selective removal of sacrificial fibers, *Biomaterials* 29 (2008) 2348–2358.
- [48] D.I. Zeugolis, S.T. Khew, E.S. Yew, A.K. Ekaputra, Y.W. Tong, L.Y. Yung, D.W. Huttmacher, C. Sheppard, M. Raghunath, Electro-spinning of pure collagen nano-fibres – just an expensive way to make gelatin?, *Biomaterials* 29 (2008) 2293–2305.
- [49] T.P. Driscoll, N.L. Nerurkar, N.T. Jacobs, D.M. Elliott, R.L. Mauck, Fiber angle and aspect ratio influence the shear mechanics of oriented electrospun nanofiber scaffolds, *J. Mech. Behav. Biomed. Mater.* 4 (2011) 1627–1636.
- [50] N.L. Nerurkar, D.M. Elliott, R.L. Mauck, Mechanics of oriented electrospun nanofiber scaffolds for annulus fibrosus tissue engineering, *J. Orthop. Res.* 25 (2007) 1018–1028.
- [51] F.J. O'Brien, *Biomaterials & scaffolds for tissue engineering*, *Mater. Today* 14 (2011) 88–95.
- [52] T.P. Green, M.A. Adams, P. Dolan, Tensile properties of the annulus fibrosus II. Ultimate tensile strength and fatigue life, *Eur. Spine J.* 2 (1993) 209–214.
- [53] T.H. McGavack, K.Y. Kao, The influence of age and sex on the soluble collagen, insoluble collagen and elastin of rat tissues, *Exp. Med. Surg.* 18 (1960) 104–123.
- [54] R. Lagier, B. Exer, Etude de la composition chimique de tissus humains de nature conjonctive en rapport avec l'âge: derme et aponévrose de la paroi abdominale, tendon d'Achille, *Gerontology* 4 (1960) 39–59.
- [55] P. Kannus, Structure of the tendon connective tissue, *Scand. J. Med. Sci. Sports* 10 (2000) 312–320.
- [56] M. Kjaer, Role of extracellular matrix in adaptation of tendon and skeletal muscle to mechanical loading, *Physiol. Rev.* 84 (2004) 649–698.
- [57] K. Weadock, R.M. Olson, F.H. Silver, Evaluation of collagen crosslinking techniques, *Biomater. Med. Devices Artif. Organs* 11 (1983) 293–318.
- [58] S. Ibusuki, G.J. Halbesma, M.A. Randolph, R.W. Redmond, I.E. Kochevar, T.J. Gill, Photochemically cross-linked collagen gels as three-dimensional scaffolds for tissue engineering, *Tissue Eng.* 13 (2007) 1995–2001.
- [59] H. Rich, M. Odlyha, U. Cheema, V. Mudera, L. Bozec, Effects of photochemical riboflavin-mediated crosslinks on the physical properties of collagen constructs and fibrils, *J. Mater. Sci. - Mater. Med.* 25 (2014) 11–21.
- [60] N.S. Tan, T. Alekseeva, R.A. Brown, Roofed grooves: rapid layer engineering of perfusion channels in collagen tissue models, *J. Biomater. Appl.* 29 (2014) 605–616.

- [61] F.P. Melchels, B. Tonnarelli, A.L. Olivares, I. Martin, D. Lacroix, J. Feijen, D.J. Wendt, D.W. Grijpma, The influence of the scaffold design on the distribution of adhering cells after perfusion cell seeding, *Biomaterials* 32 (2011) 2878–2884.
- [62] S. Lin, G. Lu, S. Liu, S. Bai, X. Liu, Q. Lu, B. Zuo, D.L. Kaplan, H. Zhu, Nanoscale control of silks for nanofibrous scaffold formation with improved porous structure, *J. Mater. Chem. B Mater. Biol. Med.* 2 (2014) 2622–2633.
- [63] S.S. Kim, C.A. Sundback, S. Kaihara, M.S. Benvenuto, B.S. Kim, D.J. Mooney, J.P. Vacanti, Dynamic seeding and in vitro culture of hepatocytes in a flow perfusion system, *Tissue Eng.* 6 (2000) 39–44.
- [64] D. Wendt, A. Marsano, M. Jakob, M. Heberer, I. Martin, Oscillating perfusion of cell suspensions through three-dimensional scaffolds enhances cell seeding efficiency and uniformity, *Biotechnol. Bioeng.* 84 (2003) 205–214.
- [65] L.A. Solchaga, E. Tognana, K. Penick, H. Baskaran, V.M. Goldberg, A.I. Caplan, J.F. Welter, A rapid seeding technique for the assembly of large cell/scaffold composite constructs, *Tissue Eng.* 12 (2006) 1851–1863.
- [66] J.F. Alvarez-Barreto, S.M. Linehan, R.L. Shambaugh, V.I. Sikavitsas, Flow perfusion improves seeding of tissue engineering scaffolds with different architectures, *Ann. Biomed. Eng.* 35 (2007) 429–442.
- [67] T.S. Karande, J.L. Ong, C.M. Agrawal, Diffusion in musculoskeletal tissue engineering scaffolds: design issues related to porosity, permeability, architecture, and nutrient mixing, *Ann. Biomed. Eng.* 32 (2004) 1728–1743.
- [68] G. Chang, H.J. Kim, G. Vunjak-Novakovic, D.L. Kaplan, R. Kandel, Enhancing annulus fibrosus tissue formation in porous silk scaffolds, *J. Biomed. Mater. Res. A* 92 (2010) 43–51.